Vibration analysis of a bowed string involving dynamics of a soundbox and neck and its application to a Chinese traditional bowed string instrument "Erhu"

Samejima, Toshiya
Faculty of Design, Kyushu University

出版情報：Acoustical Science and Technology. 44 (3), pp.281-291, 2023-05-01. 日本音響学会
バージョン：

Acoust. Sci. & Tech. **44**, 3 (2023)

PAPER

Vibration analysis of a bowed string involving dynamics of a soundbox and neck and its application to a Chinese traditional bowed string instrument "Erhu"

Toshiya Samejima*

Faculty of Design, Kyushu University,
4–9–1 Shiobaru, Minami-ku, Fukuoka, 815–8540 Japan

(*Received 28 May 2022, Accepted for publication 22 December 2022*)

Abstract: In this paper, the author extends existing analysis methods for bowed string vibration to that involving the dynamics of a soundbox and neck of a bowed string instrument. Almost all the components of the instrument such as strings, nut, tuning pegs, neck, soundbox, and bridge are physically modeled and numerically analyzed by the finite element method, thereby yielding an equation of motion of the total multi-degree-of-freedom (MDOF) system. Then, the MDOF system is introduced into an existing equivalent circuit representation of the vibrations of a bowed string. The developed method is applied to the physical modeling sound synthesis of the erhu, a Chinese traditional bowed string instrument. Trial numerical calculations demonstrate that the developed method is effective in the sound synthesis of the erhu and also has the potential to analyze the three-dimensional spatial vibration of a bowed string and the effect of the interaction between the string and soundbox vibrations.

Keywords: Violin, Erhu, Helmholtz wave, Equivalent circuit, Finite element method, Boundary element method, Finite difference method

1. INTRODUCTION

The vibration of a bowed string has been modeled by Kishi *et al.* as an equivalent circuit based on an electrical impedance analogy (the force–voltage method) for the stick-slip motion of the string [1,2]. This analysis method models the violin bow as a perfectly inelastic structural element, i.e., it has infinite internal impedance in the equivalent circuit. The string is modeled as a flexible ideal string with fixed ends.

By using the finite element method (FEM) to analyze a vibration field of the violin bow, and combining this FEM analysis with the bowed string vibration equivalent circuit representation proposed by Kishi *et al.*, the author of this paper previously constructed a model that couples the bowed string vibration and the vibration of the bow to simulate the total vibration field [3].

In this study, the author attempts to improve the analysis method for bowed string vibration by shifting the viewpoint to the string, sound box, and neck, instead of the bow. Specifically, an analytical model of the vibration field of the string, sound box, and neck using the FEM is introduced into the equivalent circuit representation of the bowed string vibration. As an example of the application of the developed method, the author will attempt to synthesize the physical modeling sound of the erhu, a Chinese traditional bowed string instrument.

2. EXISTING ANALYSIS METHODS

2.1. Bowed String Vibration Equivalent Circuit by Kishi *et al.*

The equivalent circuit model of bowed string vibration proposed by Kishi *et al.* is shown in Fig. 1 [1,2]. The potential difference across the terminal pair B-B′ represents the bow position on the string bowed by the bow; the position moves at the constant speed v_{B}. This is equivalent to a constant current source. A nonlinear resistance, r_{N}, representing the frictional characteristics between the bow and the string, is inserted between the terminal pairs B-B′ and S-S′. As modeled in Ref. [1], this resistance has a frictional nature shown in Fig. 2; this can be expressed by the following equation:

*e-mail: samejima@design.kyushu-u.ac.jp
[doi:10.1250/ast.44.281]

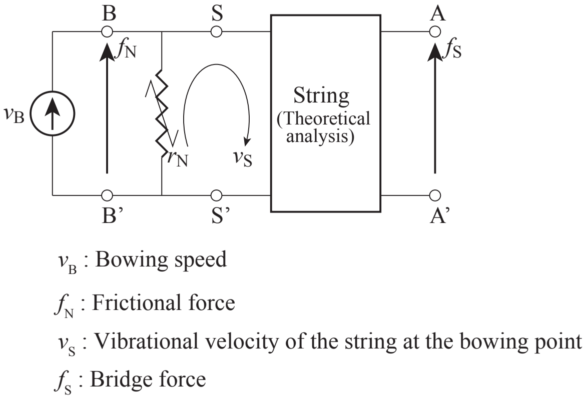

Fig. 1 Electrical equivalent circuit of a bowed string proposed by Kishi *et al.* [1,2].

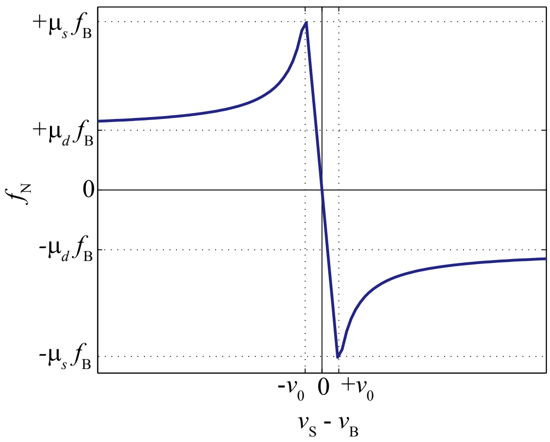

Fig. 2 Bow friction characteristics.

$$\frac{f_N}{f_B} = \begin{cases} \mu_d - \dfrac{(\mu_s - \mu_d)v_0}{v_S - v_B} & (v_S - v_B < -v_0) \\ \dfrac{-\mu_s}{v_0}(v_S - v_B) & (v_0 \leq v_S - v_B < +v_0) \\ -\mu_d - \dfrac{(\mu_s - \mu_d)v_0}{v_S - v_B} & (+v_0 \leq v_S - v_B). \end{cases} \tag{1}$$

Here, f_N is the frictional force (driving force applied to the string) generated by r_N, f_B is the bowing force (bowing pressure), μ_s and μ_d are constants giving the maximum and minimum coefficients of friction, respectively, and v_0 is the velocity for determining frictional characteristics.

The string is represented on the right from terminal S-S′; in the black box, a theoretical analysis of the string vibration is implemented using the modal expansion method. Note that v_S is the vibrational velocity of the string at the bowing point on the string. Across the terminal A-A′, the equivalent circuit outputs the force f_S exerted by the string on the bridge of the instrument as the string vibrates transversely.

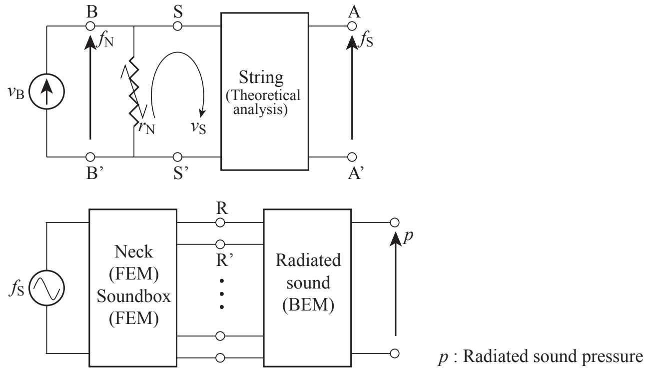

Fig. 3 Electrical equivalent circuit of the bowed string (above) and that of the vibro-acoustic field of body (below) proposed in the author's previous paper [4].

2.2. Finite Element and Boundary Element Analyses of Soundbox, Neck, and Radiated Sound Field

Figure 3 shows the equivalent circuit of the physical modeling sound synthesis method for bowed string instruments, already proposed by the author in Ref. [4]. Using the bowed string vibration equivalent circuit described in Sect. 2.1, the bridge force f_S is calculated in advance for the input into the vibro-acoustic field described below.

The soundbox of a bowed string instrument is physically modeled as a shell vibration field and the neck as a beam vibration field, and these are correctly coupled, then numerically analyzed by the FEM. This analysis part is the same as the proposed analysis method in this paper, thus a detailed mathematical expression is not given here but will be given in the next section.

The governing equation for the radiated sound field around a bowed string instrument is the wave equation for the velocity potential ϕ. The soundbox, i.e., the shell, is considered as a thin obstacle that affects the surrounding sound field. In this case, the wave equation related to ϕ can be analyzed using the integral equation derived from the normally differentiated Kirchhoff–Huygens formula, which can be used to efficiently analyze acoustic scattering from a thin obstacle. Let us consider the sound field around a thin, impenetrable obstacle, as shown in Fig. 4. According to Terai [5,6], the velocity potential ϕ at the receiving point $\boldsymbol{r}_p$ in the exterior domain Ω can be calculated using the following formula:

$$\phi(\boldsymbol{r}_p) = \iint_\Gamma \tilde{\phi}(\boldsymbol{r}_q) \frac{\partial G(\boldsymbol{r}_q, \boldsymbol{r}_p)}{\partial \boldsymbol{n}_q} dS_q, \quad \boldsymbol{r}_p \in \Omega, \tag{2}$$

where $G(\boldsymbol{r}_q, \boldsymbol{r}_p)$ is the free-space three-dimensional Green's function and $\tilde{\phi}$ is the jump discontinuity of ϕ across the obstacle. If $\boldsymbol{r}_p$ converges to the point on the surface Γ of one side of the obstacle and Eq. (2) is differentiated with respect to the outward normal $\boldsymbol{n}_p$ at $\boldsymbol{r}_p$, the following integral equation is obtained:

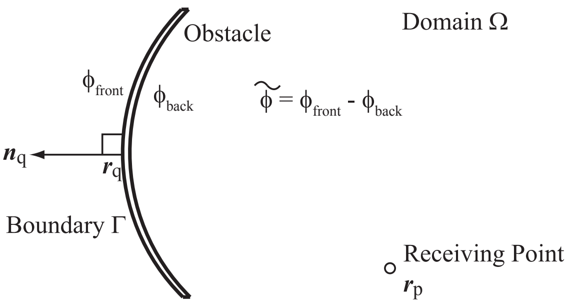

Fig. 4 Sound field around a thin obstacle.

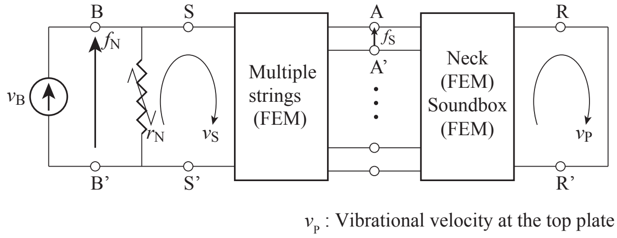

Fig. 5 Electrical equivalent circuit of a bowed string involving dynamics of a soundbox and neck proposed in this paper.

$$\frac{\partial \phi(\boldsymbol{r}_{\mathrm{p}})}{\partial \boldsymbol{n}_{\mathrm{p}}} = \iint_{\Gamma} \tilde{\phi}(\boldsymbol{r}_{\mathrm{q}}) \frac{\partial^2 G(\boldsymbol{r}_{\mathrm{q}}, \boldsymbol{r}_{\mathrm{p}})}{\partial \boldsymbol{n}_{\mathrm{p}} \partial \boldsymbol{n}_{\mathrm{q}}} dS_{\mathrm{q}}, \quad \boldsymbol{r}_{\mathrm{p}} \in \Gamma. \tag{3}$$

Given the normal component of acoustic particle velocity $v_{\mathrm{n}} = -\partial\phi(\boldsymbol{r}_{\mathrm{p}})/\partial \boldsymbol{n}_{\mathrm{p}}$ on the obstacle surface as a boundary condition, Eq. (3) can be written as an equation in terms of the unknowns $\tilde{\phi}(\boldsymbol{r}_{\mathrm{p}})$. To solve this equation, we apply the boundary element method (BEM). Discretizing the surface Γ of one side of the obstacle into N boundary elements yields a matrix equation:

$$\boldsymbol{A}\tilde{\boldsymbol{\phi}} = \boldsymbol{v}, \tag{4}$$

where $\tilde{\boldsymbol{\phi}}$ is a vector with components of $\tilde{\phi}(\boldsymbol{r}_{\mathrm{q}})$ at each node and $\boldsymbol{v}$ is a vector with components of the normal component of acoustic particle velocity $v_{\mathrm{n}}(\boldsymbol{r}_{\mathrm{q}})$ at each node. Once the values of $\tilde{\phi}(\boldsymbol{r}_{\mathrm{q}})$ are obtained by solving Eq. (4), one can calculate $\phi(\boldsymbol{r}_{\mathrm{p}})$ at an arbitrary receiving point $\boldsymbol{r}_{\mathrm{p}}$ in the domain Ω using a discretized version of the right-hand side of Eq. (2).

The shell vibration field and radiated sound field are linked together through the continuity of the pressure and velocity at the interface between the shell and the fluid. First, the transverse applied force per unit area to the shell is given by the jump discontinuity of the pressure across the shell, which is easily calculated using $\tilde{\phi}$. Second, the normal component of acoustic particle velocity at the surface of the shell is equal to the transverse velocity of the shell. As a result, the system is expressed as a fully coupled vibro-acoustic system. The pre-calculated f_{S} is used to drive this coupled system, thereby synthesizing the sound radiated from the bowed string instrument. Note that the string vibration and this coupled vibro-acoustic system (the shell vibration and radiated sound) are dealt with separately, i.e., not coupled. Hence, the author's previous method displayed in Fig. 3 cannot be used to analyze the effect of the interaction between the string and soundbox vibrations.

3. PROPOSED ANALYSIS METHOD

The equivalent circuit of the newly proposed bowed string vibration analysis method is shown in Fig. 5. Instead of the theoretical analysis of the transverse vibration of a single string based on the modal expansion method, the FEM is used for the numerical analysis of the three-dimensional vibration of multiple strings. The multiple strings will be connected to the soundbox and neck at several points, such as the nut, bridge, and tailpiece. Therefore, the black box for the multiple strings and that for the soundbox and neck are joined through multiple terminals indicated by "A-A′ ..." in the figure. Several of those terminals correspond to the terminals to which the forces f_{S} exerted by the strings on the bridge, i.e., bridge forces, are applied. In this way, the string FEM model constructs a fully coupled system with the FEM model of the soundbox and neck. The circuit is driven by the frictional force f_{N} shown in Fig. 2. Note that the proposed method does not involve an acoustic field as a starting point. The interaction between the structural vibration and the acoustic field is left for future research.

As an example of the application of the proposed analysis method, the Chinese traditional bowed string instrument called an erhu, which is shown in Fig. 6, is introduced in this paper. In the figure, for each element, its Chinese character is also displayed. The erhu has two strings called the inner and outer strings, which are generally tuned to D4 and A4, respectively. The bow hair is passed between the two strings, and the player sits with the erhu on his/her left thigh. The soundbox is made of pterocarpus, ebony, or sandalwood. Over the front of the soundbox, the python skin is stretched. The back of the soundbox is open and decorated with a lattice-work. Most soundboxes are hexagonal but octagonal and circular ones also exist. The string vibrations excited by bowing with a bow are transmitted to the python skin via the bridge, and the python skin vibrations lead to acoustic radiation. Another feature of the erhu not found in other instruments is the noise suppressor. The noise suppressor is generally made of felt or sponge, and it suppresses the generation of wolf tone, which is generally considered as noise. The erhu is a stringed instrument like the violin, but because of these differences in instrument structure, it has a unique tone that is not found in the violin.

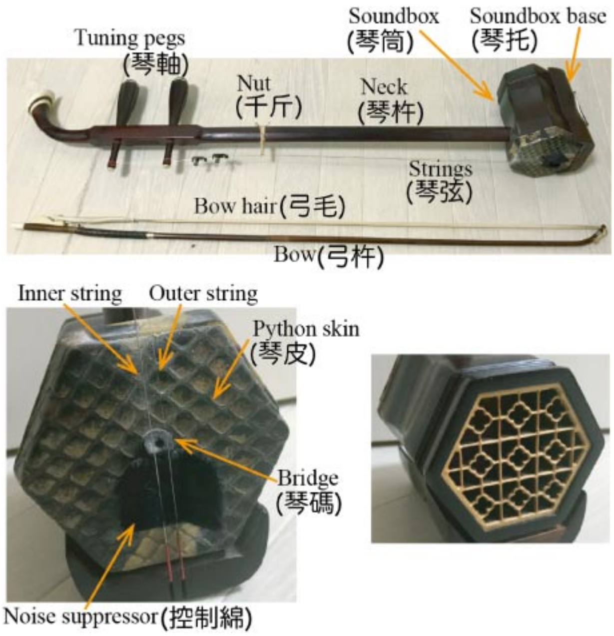

Fig. 6 Components of an erhu.

In a previous study related to the acoustic vibration analysis of the erhu, Waltham proposed a simple physical model, in which the soundbox is regarded as a cylindrical closed tube, and compared the results of his calculations with those of actual measurements [7]. Taguti modeled the python skin as isotropic and anisotropic elastic materials, analyzed their eigenmodes, and measured the acoustic vibration of the python skin [8,9]. However, no studies have been conducted on the detailed physical modeling of structural components or the coupled analysis of the vibration fields of structures and bowed string vibrations.

In this section, each appropriate physical model of each component of an erhu is given. Their governing equations and numerical analysis methods are described in detail.

3.1. Physical Model of Strings, Nut, Tuning Pegs, and Neck

Figure 7 shows the constituent elements of erhu and the respective physical models. The strings and nut are physically modeled as beams subjected to tension T_{S}. This physical model involves flexural, transverse or bending waves, quasi-longitudinal waves, and torsional vibrations at the same time.

Let ξ_{S}, η_{S}, ζ_{S}, and $\theta_{x\mathrm{S}}$ be the vibrational displacements in the x_{S}-, y_{S}-, and z_{S}-axes, and the angle of rotation around the x_{S}-axis of a beam with length in the x_{S}-axis direction, respectively; $(x_{\mathrm{S}}, y_{\mathrm{S}}, z_{\mathrm{S}})$ denotes the local coordinate system for the string. Then, the respective governing equations are expressed as

$$\rho_{\mathrm{S}} S \frac{\partial^2 \xi_{\mathrm{S}}}{\partial t^2} = E_{\mathrm{S}} S \frac{\partial^2 \xi_{\mathrm{S}}}{\partial x_{\mathrm{S}}^2} - R_{x\mathrm{S}} \frac{\partial \xi_{\mathrm{S}}}{\partial t}, \tag{5}$$

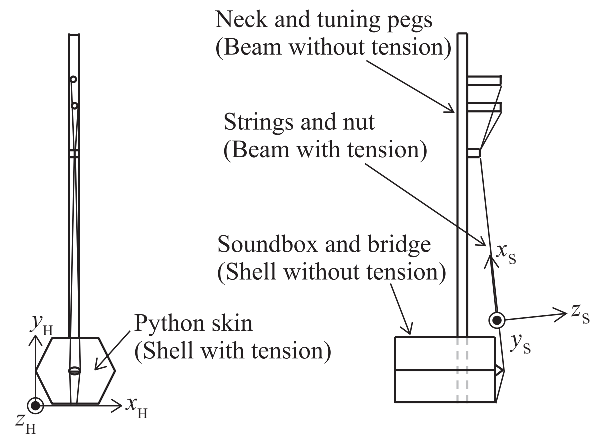

Fig. 7 Physical model of an erhu.

$$\rho_{\mathrm{S}} S \frac{\partial^2 \eta_{\mathrm{S}}}{\partial t^2} = T_{\mathrm{S}} \frac{\partial^2 \eta_{\mathrm{S}}}{\partial x_{\mathrm{S}}^2} - E_{\mathrm{S}} I_{z\mathrm{S}} \frac{\partial^4 \eta_{\mathrm{S}}}{\partial x_{\mathrm{S}}^4} - R_{y\mathrm{S}} \frac{\partial \eta_{\mathrm{S}}}{\partial t} + \epsilon_{\mathrm{S}} f_{y\mathrm{S}}, \tag{6}$$

$$\rho_{\mathrm{S}} S \frac{\partial^2 \zeta_{\mathrm{S}}}{\partial t^2} = T_{\mathrm{S}} \frac{\partial^2 \zeta_{\mathrm{S}}}{\partial x_{\mathrm{S}}^2} - E_{\mathrm{S}} I_{y\mathrm{S}} \frac{\partial^4 \zeta_{\mathrm{S}}}{\partial x_{\mathrm{S}}^4} - R_{z\mathrm{S}} \frac{\partial \zeta_{\mathrm{S}}}{\partial t} + \epsilon_{\mathrm{S}} f_{z\mathrm{S}}, \tag{7}$$

$$\rho_{\mathrm{S}} S I_{\mathrm{pS}} \frac{\partial^2 \theta_{x\mathrm{S}}}{\partial t^2} = G_{\mathrm{S}} I_{\mathrm{pS}} \frac{\partial^2 \theta_{x\mathrm{S}}}{\partial x_{\mathrm{S}}^2} - R_{\mathrm{p}} \frac{\partial \theta_{x\mathrm{S}}}{\partial t}, \tag{8}$$

with

$$\epsilon_{\mathrm{S}}(x_{\mathrm{S}}) = \frac{f_{\mathrm{a}}(x_{\mathrm{S}})}{\displaystyle\int_L f_{\mathrm{a}}(x_{\mathrm{S}}) dx_{\mathrm{S}}},$$

where ρ_{S} is the volume density, S is the cross-sectional area, E_{S} is Young's modulus, T_{S} is the tension, $I_{z\mathrm{S}}$ and $I_{y\mathrm{S}}$ are the moments of inertia of area around the z_{S}- and y_{S}-axes, respectively, I_{pS} is the polar moment of inertia of area, $G_{\mathrm{S}} = E_{\mathrm{S}}/(2(1+\nu_{\mathrm{S}}))$ is the shear modulus, and ν_{S} is Poisson's ratio. Moreover, $R_{x\mathrm{S}}$, $R_{y\mathrm{S}}$, $R_{z\mathrm{S}}$, and R_{p} are the resistance coefficients per unit length and ϵ_{S} is the spatial distribution of the force with respect to the excitation forces $f_{y\mathrm{S}}$ and $f_{z\mathrm{S}}$. The tuning pegs and neck are physically modeled as ordinary beams without tension.

3.2. Physical Model of a Python Skin, Soundbox, and Bridge

The python skin stretched over the front surface of the body is physically modeled as a shell with tension T_{H}. Out-of-plane, in-plane, and torsional vibrations are included in the shell. If only the governing equation for the transverse vibrational displacement ζ_{H} is extracted, it is expressed as

$$\rho_{\mathrm{H}} h_{\mathrm{H}} \frac{\partial^2 \zeta_{\mathrm{H}}}{\partial t^2} = T_{\mathrm{H}} \nabla^2 \zeta_{\mathrm{H}} - D \nabla^4 \zeta_{\mathrm{H}} - R_{z\mathrm{H}} \frac{\partial \zeta_{\mathrm{H}}}{\partial t}, \tag{9}$$

where ρ_{H} is the volume density, h_{H} is the thickness, $D = E_{\mathrm{H}} h_{\mathrm{H}}^3/(12(1-\nu_{\mathrm{H}}^2))$ is the flexural rigidity, E_{H} is Young's modulus, ν_{H} is Poisson's ratio, T_{H} is the tension, and $R_{z\mathrm{H}}$ is the resistance coefficient per unit area. Operator ∇^2 denotes the Laplacian, defined in the local two-dimensional coordinates (x_H, y_H) for the python skin. Operator ∇^4 indicates a double application of the Laplacian operator, which is referred to as a bi-Laplacian or biharmonic operator. The body and bridge are physically modeled as ordinary shells without tension.

3.3. Application of the Finite Element Method

The FEM is employed for the numerical analysis of Eqs. (5)–(8), which represent the beam vibration field. Adopting a third-order beam element [10,11] that simultaneously considers transverse waves, quasi-longitudinal waves, and torsional vibrations, we obtain the following equation of motion of a multi-degree-of-freedom (MDOF) system:

$$\boldsymbol{M}_S \frac{d^2\boldsymbol{\delta}_S}{dt^2} + \boldsymbol{C}_S \frac{d\boldsymbol{\delta}_S}{dt} + \boldsymbol{K}_S\boldsymbol{\delta}_S = \boldsymbol{f}_{Sy}f_{yS} + \boldsymbol{f}_{Sz}f_{zS}, \quad (10)$$

$$\begin{Bmatrix} v_S \\ w_S \end{Bmatrix} = \boldsymbol{G}_S \frac{d\boldsymbol{\delta}_S}{dt}. \quad (11)$$

Here, $\boldsymbol{M}_S$ is the mass matrix, $\boldsymbol{C}_S$ is the damping matrix, $\boldsymbol{K}_S$ is the stiffness matrix, and $\boldsymbol{\delta}_S$ is a vector consisting of the vibrational nodal values. f_{yS} and f_{zS}, which are also used in Eqs. (6) and (7), express the excitation force applied to a bowing point per unit length along the y_S- and z_S-axes, respectively. (x_S, y_S, z_S) denotes the local coordinate system for the FEM model of the string, where x_S is the direction to which the string is stretched. $\boldsymbol{f}_{Sy}$ and $\boldsymbol{f}_{Sz}$ represent the force vectors, in which only the elements related to f_{yS} and f_{zS} remain and the values of the other elements are set to 0; then, only the coefficients of f_{yS} and f_{zS} are considered. For a more detailed procedure for constructing these characteristic matrices, the reader is referred to Refs. [10,11]. Now, let v_S and w_S be the vibrational velocities of the string in the y_S- and z_S-directions, respectively. The matrix $\boldsymbol{G}_S$ extracts the nodal values corresponding to v_S and w_S from $d\boldsymbol{\delta}_S/dt$.

For the shell vibration field, including Eq. (9), the FEM using a planar shell element [12,13] is applied. Then, the following equation of motion of the MDOF system is obtained:

$$\boldsymbol{M}_H \frac{d^2\boldsymbol{\delta}_H}{dt^2} + \boldsymbol{C}_H \frac{d\boldsymbol{\delta}_H}{dt} + \boldsymbol{K}_H\boldsymbol{\delta}_H = \boldsymbol{0}. \quad (12)$$

For a more detailed procedure for constructing the characteristic matrices, the reader is referred to Refs. [12,13].

The two FEM equations Eqs. (10) and (12) are coupled using the coupling condition that there are equal vibrational displacements at common nodal points between the beam and the shell. A method for this is Lagrange's method of indeterminate multiplier [14]. Through this method, we obtain the following equation of motion of the total MDOF system involving both the beam and shell vibration fields:

$$\boldsymbol{M} \frac{d^2\boldsymbol{\delta}}{dt^2} + \boldsymbol{C} \frac{d\boldsymbol{\delta}}{dt} + \boldsymbol{K}\boldsymbol{\delta} = \boldsymbol{F}\begin{Bmatrix} f_{yS} \\ f_{zS} \end{Bmatrix} \quad (13)$$

with

$$\boldsymbol{M} = \begin{bmatrix} \boldsymbol{M}_S & \boldsymbol{0} & \boldsymbol{0} \\ \boldsymbol{0} & \boldsymbol{M}_H & \boldsymbol{0} \\ \boldsymbol{0} & \boldsymbol{0} & \boldsymbol{0} \end{bmatrix}, \quad \boldsymbol{C} = \begin{bmatrix} \boldsymbol{C}_S & \boldsymbol{0} & \boldsymbol{0} \\ \boldsymbol{0} & \boldsymbol{C}_H & \boldsymbol{0} \\ \boldsymbol{0} & \boldsymbol{0} & \boldsymbol{0} \end{bmatrix},$$

$$\boldsymbol{K} = \begin{bmatrix} \boldsymbol{K}_S & \boldsymbol{0} & \boldsymbol{L}_S^T \\ \boldsymbol{0} & \boldsymbol{K}_H & -\boldsymbol{L}_H^T \\ \boldsymbol{L}_S & -\boldsymbol{L}_H & \boldsymbol{0} \end{bmatrix},$$

$$\boldsymbol{F} = \begin{bmatrix} \boldsymbol{f}_{Sy} & \boldsymbol{f}_{Sz} \\ \boldsymbol{0} & \boldsymbol{0} \\ \boldsymbol{0} & \boldsymbol{0} \end{bmatrix}, \quad \boldsymbol{\delta} = \begin{Bmatrix} \boldsymbol{\delta}_S \\ \boldsymbol{\delta}_H \\ \boldsymbol{\lambda} \end{Bmatrix}.$$

Here, $\boldsymbol{\lambda}$ is a vector consisting of Lagrange's indeterminate multipliers for the constrained condition that the vibrational nodal values of the beam elements equal those of the shell elements at common nodal points. The matrices $\boldsymbol{L}_S$ and $\boldsymbol{L}_H$ extract the common nodal values from $\boldsymbol{\delta}_S$ and $\boldsymbol{\delta}_H$, respectively.

3.4. Coupling with Bow Friction Characteristics

Let us consider the case where the bowing direction $\widehat{y}$ is inclined by $\theta + \pi$ with respect to y_S, as shown in Fig. 8. In this case, the vibrational velocities $\widehat{v_S}$ and $\widehat{w_S}$ in the $\widehat{y}$- and $\widehat{z}$-directions, respectively, can be given by

$$\begin{Bmatrix} \widehat{v_S} \\ \widehat{w_S} \end{Bmatrix} = \begin{bmatrix} \cos(\theta+\pi) & \sin(\theta+\pi) \\ -\sin(\theta+\pi) & \cos(\theta+\pi) \end{bmatrix} \begin{Bmatrix} v_S \\ w_S \end{Bmatrix}. \quad (14)$$

If we regard $\widehat{v_S}$ as the vibrational velocity v_S of the string at the bowing point in Eq. (1), we can obtain the frictional force (driving force applied to the string) f_N at a given bowing force (bowing pressure) f_B from the relation in Eq. (1). Once f_N and f_B are determined, the required f_{yS} and f_{zS} values for the calculation in Eq. (12) can be obtained using the following formula:

$$\begin{Bmatrix} f_{yS} \\ f_{zS} \end{Bmatrix} = \begin{bmatrix} \cos(\theta+\pi) & -\sin(\theta+\pi) \\ \sin(\theta+\pi) & \cos(\theta+\pi) \end{bmatrix} \begin{Bmatrix} f_N \\ f_B \end{Bmatrix}. \quad (15)$$

4. NUMERICAL EXAMPLE

4.1. Calculation Conditions

Figure 9 illustrates the FEM mesh model created for the erhu in Fig. 6. The support conditions are completely fixed (indicated by "Clamped" in the figure) in terms of the position of the neck held by the left hand and the position of the soundbox placed on the left thigh. The function $f_a(x_S)$ used in the spatial distribution of the force ϵ_S in Eqs. (6) and (7) was given by the Dirac delta function,

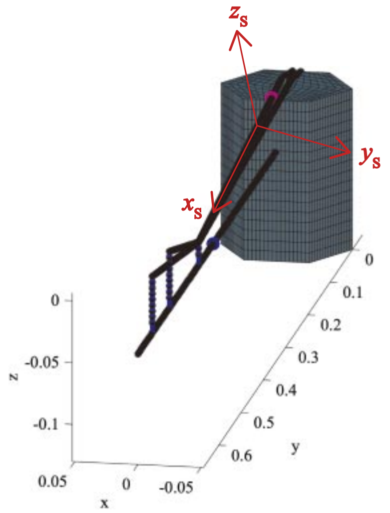

(a) Local coordinate system (x_S, y_S, z_S) for the FEM model of the string

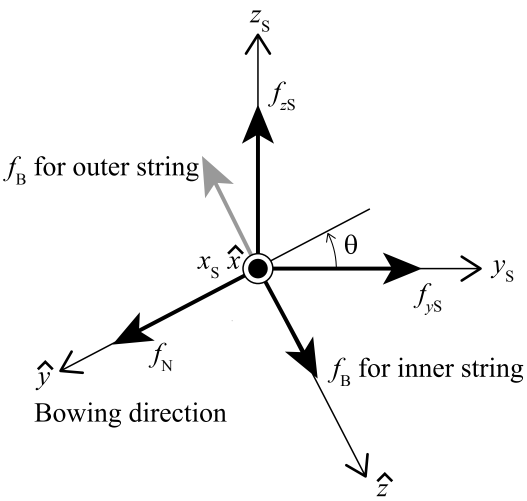

(b) Bowing direction $\hat{y}$ and bowing force (bowing pressure) direction $\hat{z}$

Fig. 8 Geometrical arrangement of the bowing direction and strings.

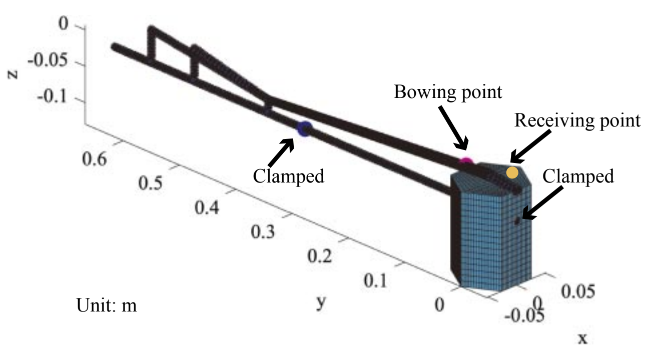

Fig. 9 Finite element model of the erhu; (x, y, z) denotes the global coordinate system.

selecting the location of the "bowing point" in the figure. The physical properties of the materials given in Tables 1 and 2 are based on Refs. [7–9]. The damping of the total system was assumed to be proportional viscous damping and given by $\boldsymbol{C} = 10^{-4}\boldsymbol{K}$ in Eq. (13).

Table 1 Geometric and material properties of the erhu used in the calculation: beams.

Parameters	Values
For neck	
Semimajor axis of ellipse	10.5×10^{-3} m
Semiminor axis of ellipse	7.50×10^{-3} m
Young's modulus: E_N	12.4 GPa
Poisson's ratio: ν_N	0.35
Density: ρ_N	1,050 kg/m^3
Moments of inertia of area: I_{zN}	3.479×10^{-9} m^4
I_{yN}	6.819×10^{-9} m^4
Polar moment of inertia of area: I_{pN}	9.741×10^{-9} m^4
For tuning pegs	
Diameter of section	10.0×10^{-3} m
Young's modulus: E_N	12.4 GPa
Poisson's ratio: ν_N	0.35
Density: ρ_N	1,050 kg/m^3
Moments of inertia of area: I_{zN}, I_{yN}	4.909×10^{-10} m^4
Polar moment of inertia of area: I_{pN}	9.818×10^{-10} m^4
For inner string	
Diameter of section	0.440×10^{-3} m
Tension: T_S	51.68 N
Young's modulus: E_S	200 GPa
Poisson's ratio: ν_S	0.35
Density: ρ_S	6,577 kg/m^3
Moments of inertia of area: I_{zS}, I_{yS}	1.840×10^{-15} m^4
Polar moment of inertia of area: I_{pS}	3.680×10^{-15} m^4
For outer string	
Diameter of section	0.260×10^{-3} m
Tension: T_S	51.50 N
Young's modulus: E_S	200 GPa
Poisson's ratio: ν_S	0.35
Density: ρ_S	8,363 kg/m^3
Moments of inertia of area: I_{zS}, I_{yS}	2.243×10^{-16} m^4
Polar moment of inertia of area: I_{pS}	4.486×10^{-16} m^4
For nut	
Semimajor axis of ellipse	7.50×10^{-3} m
Semiminor axis of ellipse	6.00×10^{-3} m
Tension: T_S	9.786 N
Young's modulus: E_S	20.0 GPa
Poisson's ratio: ν_S	0.35
Density: ρ_S	7.074 kg/m^3
Moments of inertia of area: I_{zS}	1.272×10^{-9} m^4
I_{yS}	1.988×10^{-9} m^4
Polar moment of inertia of area: I_{pS}	3.181×10^{-9} m^4

The discretization of the beam vibration field involved third-order beam elements [10,11] with 579 elements and 578 nodes, and that of the shell vibration field involved planar shell elements [12,13] with 2,050 elements and 2,103 nodes. The time evolution was calculated using the finite difference method (FDM); the scheme used is the

Table 2 Geometric and material properties of the erhu used in the calculation: shells.

Parameters	Values
For sound box	
Young's modulus: E_B	12.4 GPa
Poisson's ratio: ν_B	0.35
Density: ρ_B	1,050 kg/m^3
Thickness: h_B	8×10^{-3} m
For bridge	
Young's modulus: E_B	11.8 GPa
Poisson's ratio: ν_B	0.35
Density: ρ_B	600.0 kg/m^3
Thickness: h_B	6×10^{-3} m
For python skin	
Young's modulus: E_H	2.00 GPa
Poisson's ratio: ν_H	0.35
Density: ρ_H	700.0 kg/m^3
Thickness: h_H	0.8×10^{-3} m
Tension: T_H	1,176 N/m

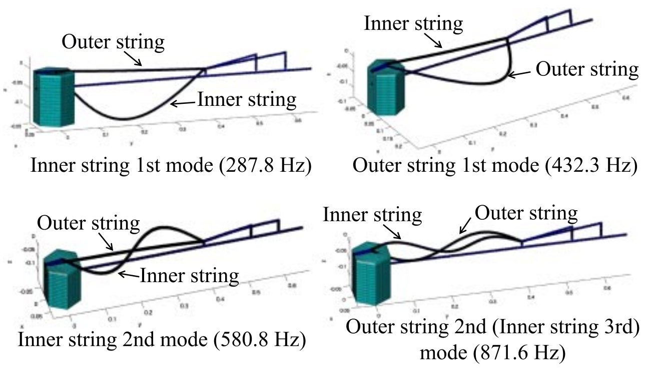

Fig. 10 Eigenfrequencies and eigenmode shapes where the strings play an active role.

explicit Runge–Kutta formula proposed by Dormand and Prince [15].

4.2. Simple Verification by Eigenmode Analysis

Before calculating time responses, the eigenmode analysis of the FEM model was performed to briefly verify the author's self-made C++ code implementing the proposed numerical method. Figures 10 and 11 show a few examples of eigenfrequencies and eigenmode shapes. The eigenmodes obtained by the calculations are a composite combination of the vibrations of the strings, nut, tuning pegs, neck, python skin, soundbox, and bridge. However, by visually observing the eigenmode shapes, the author extracted the modes that are mainly caused by the strings or python skin.

The eigenfrequency of the inner string 1st mode and that of the outer string 1st mode are very close to the pitch of D4 (293 Hz) and that of A4 (440 Hz), respectively. In

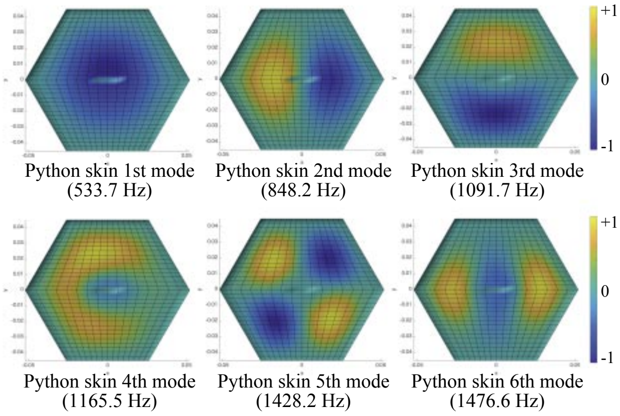

Fig. 11 Eigenfrequencies and eigenmode shapes where the python skin plays an active role.

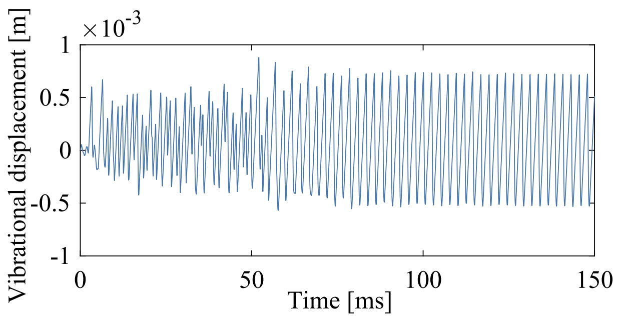

(a) Time history of the vibrational displacement

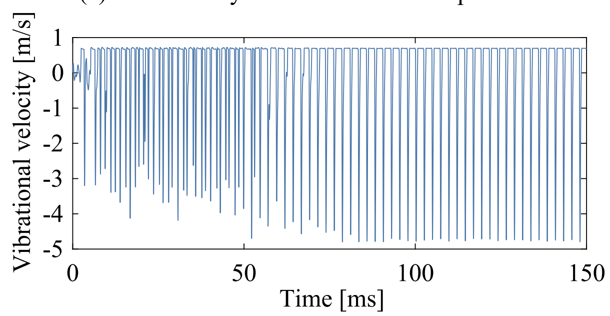

(b) Time history of the vibrational velocity

Fig. 12 Transitional time response of the bowed outer string (A4) at the bowing point calculated by the proposed method.

addition, the eigenmode shapes of the 1st, 2nd, and 3rd modes are similar to typical mode shapes of a flexible string fixed at both ends, i.e., they indicate physically reasonable shapes. As for the python skin modes, some modes close to those in the literature [8] were obtained, but some were different owing to the consideration of the bridge, strings, or neck.

4.3. Numerical Results and Discussion

Figure 12 shows the vibrational displacement and velocity at the bowing point ($x = 0.00352$ m, $y = 0.04740$ m, $z = 0.00264$ m) shown in Fig. 9, calculated by the proposed analysis method. The figure indicates the

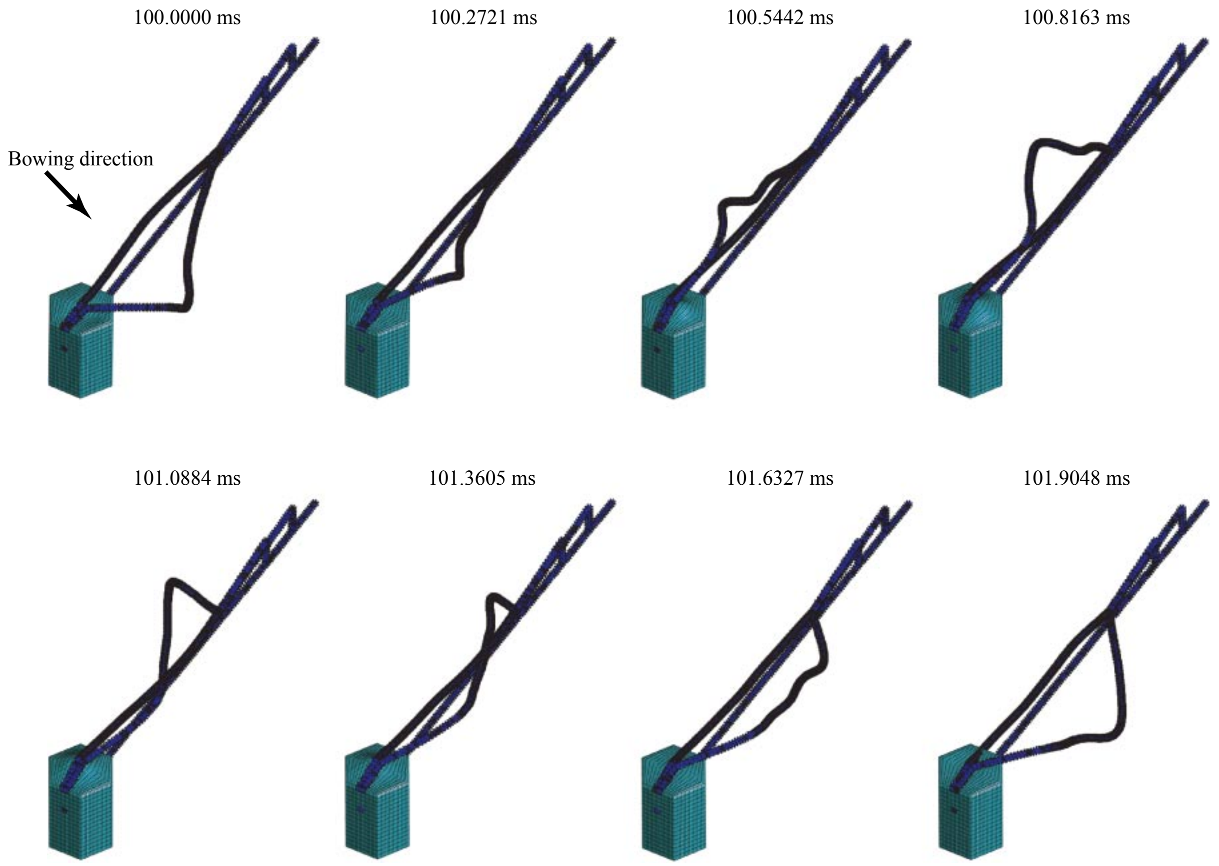

Fig. 13 Snapshots of the time evolution of the shape of the erhu model, when the outer string (A4) is bowed.

results for the outer string with the following parameters: bowing direction $\theta = 45$ degrees, bowing force $f_B = 1.46$ N (≈ 149 gw), and bowing speed $v_B = 70 \times 10^{-2}$ m/s. It can be seen that a periodic stick-slip motion is induced at around 60 ms. The upper limit of vibrational velocity at a bowing point is theoretically equal to the bowing speed; that upper limit occurs in the sticking period during which a string is carried forward by a bow. From the figure, one can observe that the vibrational velocity is nearly equal to the bowing speed of 70×10^{-2} m/s in the sticking period.

Figure 13 shows snapshots of the time development of the deformation of the erhu model. The figure also displays approximately one fundamental period of the motion from 100 ms when the oscillation becomes a completely steady state. We can see that a stationary Helmholtz wave is formed. These results indicate that the proposed analysis method can reasonably well reproduce a typical bowed string vibration.

Figure 14 illustrates the trajectory of the outer string at the bowing point in the y_S–z_S plane. One can see that a three-dimensional spatial motion arises when bowing the string. Note that existing analysis methods for bowed string vibration have not been able to reproduce such a three-dimensional spatial motion of a bowed string so far.

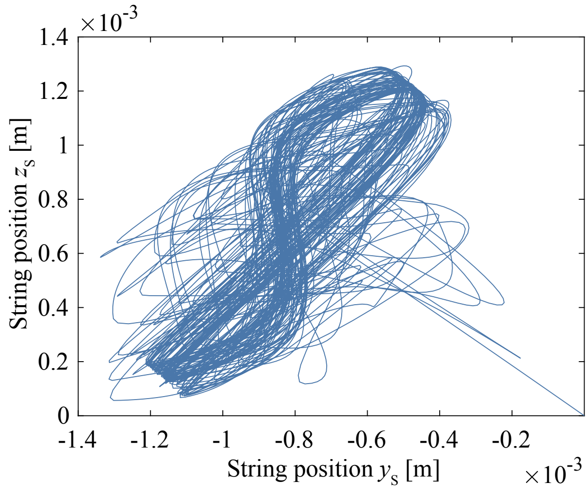

Fig. 14 Trajectory of the bowed outer string (A4) at the bowing point in the y_S–z_S plane.

Figure 15 shows the transitional time response of the vibrational velocity v_P at the receiving point ($x = 0.02356$ m, $y = -0.00844$ m, $z = 0$ m) set on the soundbox surface shown in Fig. 9, calculated by the proposed method. When this output signal was played as an audio signal, we could indeed hear a satisfactory erhu-like sound.

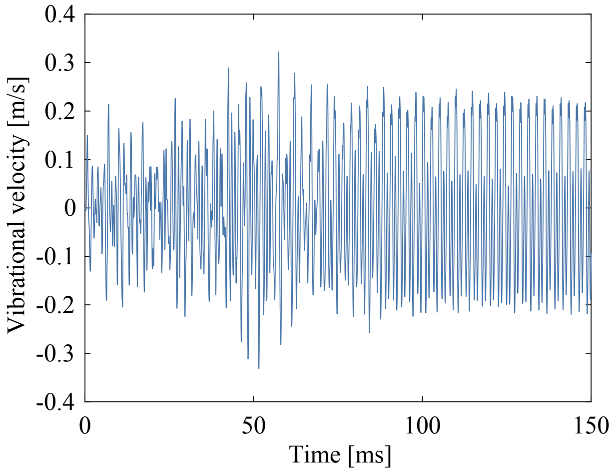

Fig. 15 Transitional time response of the vibrational velocity at the receiving point on the soundbox surface calculated by the proposed method, when the outer string (A4) is bowed.

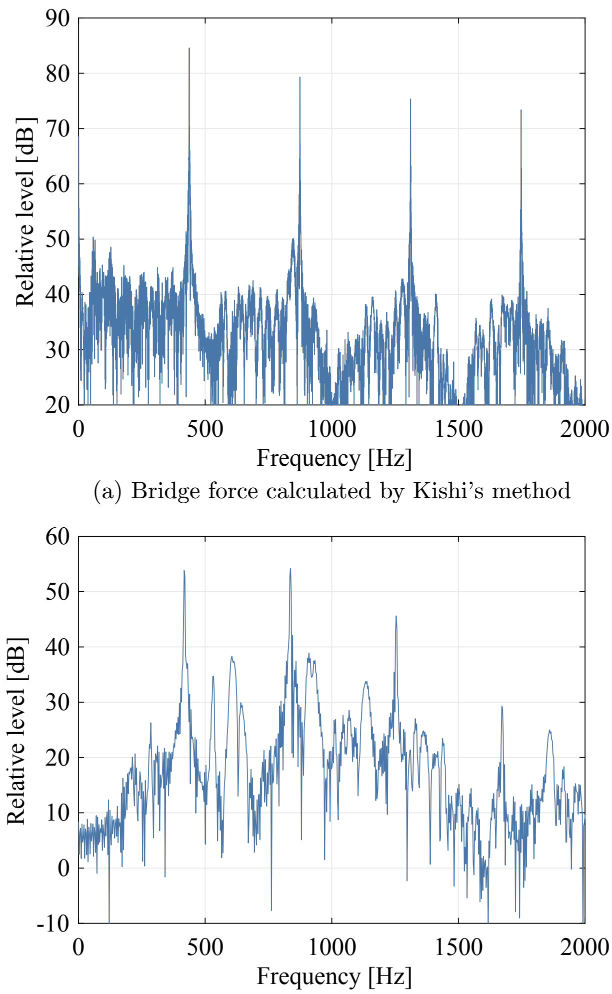

(a) Bridge force calculated by Kishi's method

(b) Vibrational velocity at the receiving point on the soundbox surface calculated by the proposed method

Fig. 16 Frequency responses of the bowing sound A4 of the erhu model.

Figure 16(a) shows the frequency characteristic of the bridge force f_S calculated using the equivalent circuit of Kishi *et al.* Figure 16(b) shows that of the vibrational velocity v_P at the receiving point set on the soundbox surface shown in Fig. 9, calculated by the proposed analysis method. Figure 16(b) demonstrates that a gradual peak is formed at 500–1,000 Hz. Several peaks caused by the python skin, soundbox, and neck are also observed, in addition to the peaks with overtone structures excited by the string. These are considered to characterize the sound of the erhu.

These numerical results described above, including the audio signal by the physical modeling synthesis, are in qualitative agreement with the real characteristics of the erhu dynamics; this fact supports, in part, the validity of the proposed analysis method. A further detailed comparison between the results of the proposed analysis method and experiment will be carried out in the next stage.

Figures 17 and 18 show the vibrational displacement and velocity at the bowing point of the inner string (D4), and the vibrational velocity v_P at the receiving point, respectively. For the condition of bowing, the same parameters as in the outer string (A4) were introduced. From the waveforms, one can observe that small periodic amplitude vibrations or beats occur. For comparison, the vibrational velocity v_P at the receiving point calculated using the author's previous method [4] is also shown in Fig. 19. In this case, the beats like those shown in Fig. 18

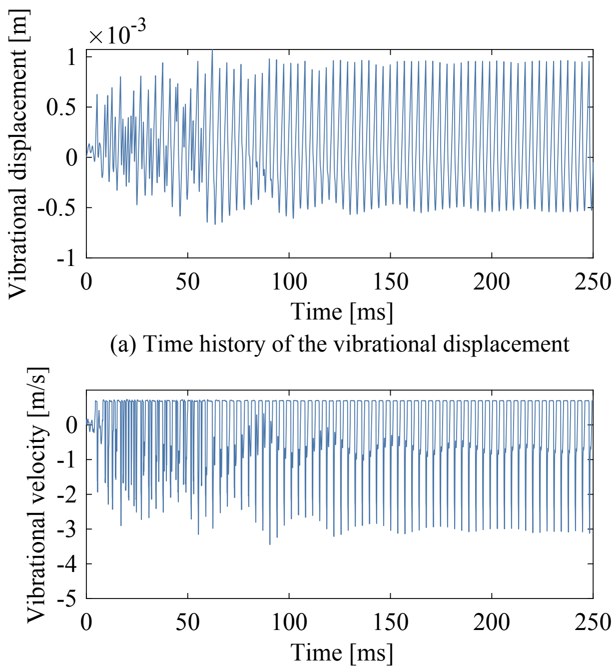

(a) Time history of the vibrational displacement

(b) Time history of the vibrational velocity

Fig. 17 Transitional time response of the bowed inner string (D4) at the bowing point calculated by the proposed method.

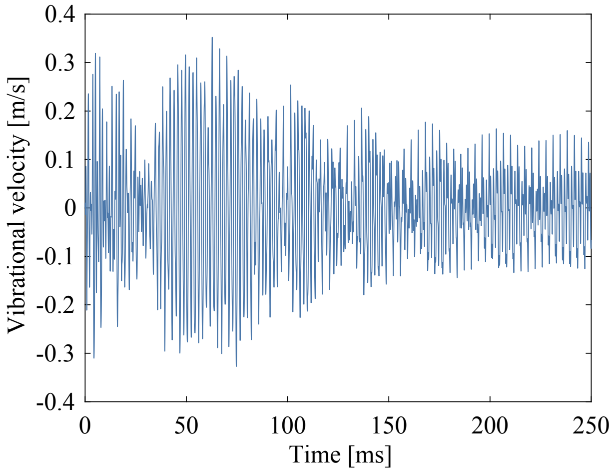

Fig. 18 Transitional time response of the vibrational velocity at the receiving point on the soundbox surface calculated by the proposed method, when the inner string (D4) is bowed.

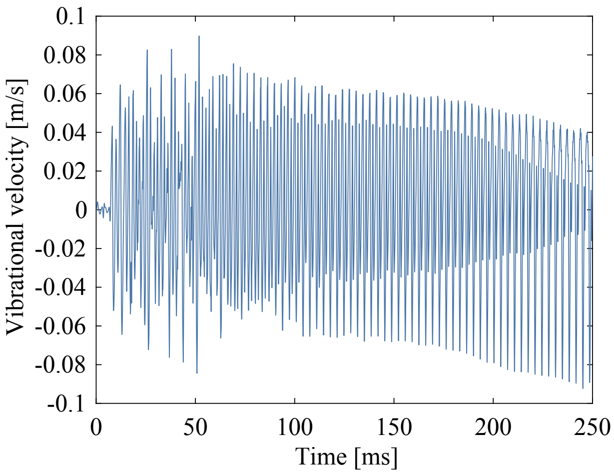

Fig. 19 Transitional time response of the vibrational velocity at the receiving point on the soundbox surface calculated by the author's previous method [4], when the inner string (D4) is bowed.

are not observed. This is probably because the author's previous method, in which the string and soundbox vibrations are not fully coupled, cannot be used to analyze the effect of the interaction between the string and soundbox vibrations.

Finally, the frequency characteristics determined by Kishi's method and the proposed analysis method, and a measured frequency response of the radiated sound of a real erhu used for the calculation model are shown in Figs. 20(a), 20(b), and 20(c), respectively. The measured frequency characteristic is considered a rough reference; a real erhu was bowed by a player in an anechoic chamber, and the output signal of a microphone placed in front of the python skin at a distance of 1 m was recorded in a PC through an audio interface. Here, since measurement

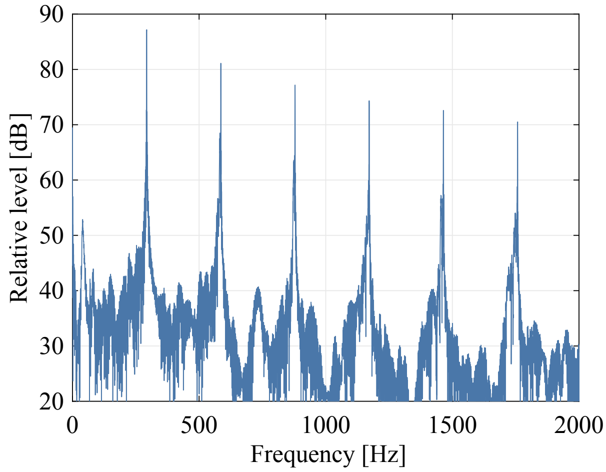

(a) Bridge force calculated by Kishi's method

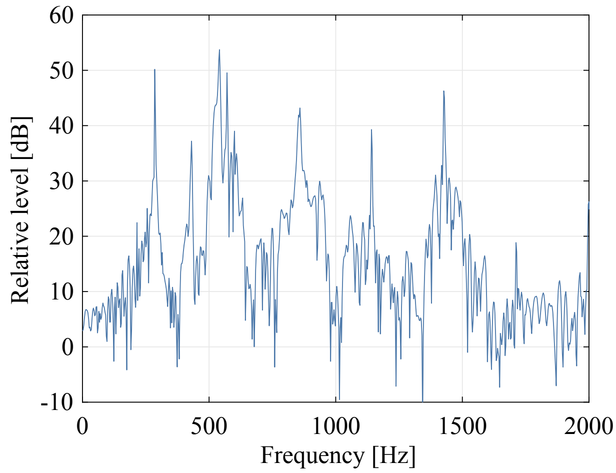

(b) Vibrational velocity at the receiving point on the soundbox surface calculated by the proposed method

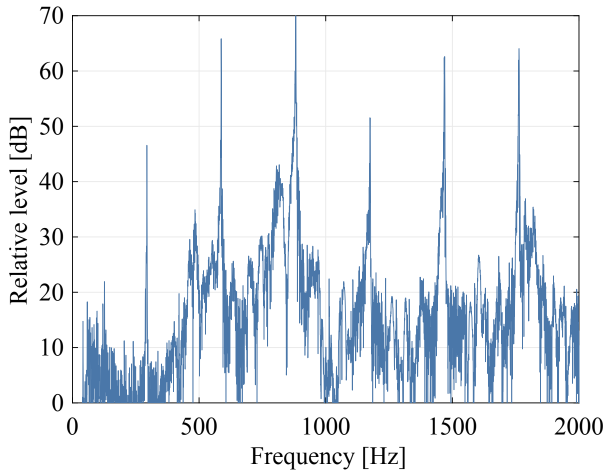

(c) Measured result of the radiated sound from a real erhu

Fig. 20 Frequency responses of the bowing sound D4 of the erhu model.

conditions were not strictly controlled, the author will not strictly compare the calculated data with the measured data. Nevertheless, roughly common frequency characteristics, such as several clear peaks in the low-frequency range can be seen in both the calculated and measured data;

this also demonstrates, in part, the validity of the developed method. Further precise measurements will be left for future work.

5. CONCLUSIONS AND FUTURE WORK

In this study, the author has attempted to improve the analysis method for bowed string vibration. In particular, the author has focused his attention on the string, sound box, and neck dynamics, and their interaction. The FEM has been employed in the numerical analysis of the vibration field of the string, sound box, and neck. All the vibration fields of these components have been fully coupled, thereby yielding an equation of motion of the total MDOF system. The MDOF system has been incorporated into the existing equivalent circuit representation of the vibrations of a bowed string. The developed method has been applied to the physical modeling sound synthesis of the erhu, a Chinese traditional bowed string instrument.

The numerical calculation results have demonstrated that the developed method can reasonably generate the Helmholtz wave, which is a typical waveform of a bowed string. In addition, the method can produce the three-dimensional spatial motion of the bowed string, which existing analysis methods for bowed string vibration have not been able to produce so far. Furthermore, it has been shown that the developed method can be used to analyze the effect of the interaction between the string and soundbox vibrations in a fully coupled state.

Future studies we should carry out are as follows:

- to further validate the proposed method, through comparing the numerical predictions with the results of experiments on a real erhu,
- to build a structure–acoustics system, i.e., to take into account the interaction between the shell vibration and its radiated sound, through acoustic scattering analysis around a thin obstacle,
- to apply the proposed method to other bowed string instruments such as violins and cellos, and
- to provide guidelines to design bowed string instruments and play them to produce their desired timbre, through the proposed numerical analysis.

ACKNOWLEDGMENT

I would like to express my gratitude to Ms. Huijia Chen for her advice on the erhu and help in creating the physical model of the sound source. This study has received funding from the Japan Society for the Promotion of Science Grants-in-Aid for Scientific Research (JSPS KAKENHI Grant Number JP19H04126).

REFERENCES

[1] K. Kishi and M. Fujio, “Digital simulation of the oscillations of the bowed string,” *Tech. Rep. Musical Acoust. Acoust. Soc. Jpn.*, **5**(2), pp. 9–16 (1986) (in Japanese).

[2] K. Kishi and T. Higashimoto, “Digital simulation of the oscillations of the bowed string,” *Proc. Spring Meet. Inst. Electron. Inf. Commun. Eng.*, 1-434–1-435 (1988) (in Japanese).

[3] T. Samejima, “Vibration analysis of a bowed string involving dynamics of a violin bow,” *J. Acoust. Soc. Jpn. (J)*, **77**, 277–287 (2021) (in Japanese).

[4] T. Samejima and E. Chin, “Physical modeling sound synthesis of a Chinese traditional bowed string instrument “Erhu”,” *Proc. Autumn Meet. Acoust. Soc. Jpn.*, pp. 1191–1194 (2021) (in Japanese).

[5] T. Terai, “On calculation of sound fields around three dimensional objects by integral equation methods,” *J. Sound Vib.*, **69**, 71–100 (1980).

[6] T. Terai, “Introduction of sound field calculation by using integral equation,” *Tech. Rep. Architect. Acoust. Acoust. Soc. Jpn.*, **AA87-05**, 1–14 (1987) (in Japanese).

[7] C. Waltham, “A simple model of the Erhu soundbox,” *Proc. 176th Meet. Acoust. Soc. Am.*, **35**, 1–13 (2018).

[8] T. Taguti, “Modal analysis on Erhu’s Qin-pi,” *Tech. Rep. Musical Acoust. Acoust. Soc. Jpn.*, **37**(4), pp. 7–12 (2018) (in Japanese).

[9] T. Taguti, “Vibro-acoustic measurement of Erhu’s Qinpi,” *Tech. Rep. Musical Acoust. Acoust. Soc. Jpn.*, **37**(6), pp. 95–100 (2018) (in Japanese).

[10] K. Washizu, H. Miyamoto, Y. Yamada, Y. Yamamoto and T. Kawai, *Yugen yousohou hand book I kiso hen* (Baihukan, Tokyo, 1981), Chap. 3, Sect. 2.7 (in Japanese).

[11] Y. Kagawa, *Yugen yousohou ni yoru shindo-onkyo kougaku/kiso to ouyou* (Baihukan, Tokyo, 1981), Sect. 5-2 (in Japanese).

[12] O. C. Zienkiewicz, *The Finite Element Method in Engineering Science* (McGraw-Hill, New York, 1971), Chap. 10, Chap. 11.

[13] K. Washizu, H. Miyamoto, Y. Yamada, Y. Yamamoto and T. Kawai, *Yugen yousohou hand book I kiso hen* (Baihukan, Tokyo, 1981), Chap. 3, Sect. 3, Sect. 4, Sect. 5.2 (in Japanese).

[14] T. Kawabe, *Analytical Dynamics for Engineering Students* (Shokabo, Tokyo, 2012), Sect. 2.6, Sect. 4.1 (in Japanese).

[15] J. R. Dormand and P. J. Prince, “A family of embedded Runge–Kutta formulae,” *J. Comput. Appl. Math.*, **6**, 19–26 (1980).

Toshiya Samejima received the B. E. and M. E. degrees from the Department of Architecture and Architectural Engineering, Waseda University, Japan, in 1992 and 1994, respectively. He received the Ph. D. degree from the Department of Architecture, the University of Tokyo, Japan, in 1997. After a period as a Research Associate at the Advanced Research Institute for Science and Engineering, Waseda University, and as a Lecturer in the Department of Acoustic Design, Kyushu Institute of Design, Japan, he is currently a Professor in the Faculty of Design, Kyushu University, Japan. His research interests are in the theoretical/numerical analysis and control of sound and vibration. He is a member of ASJ, AIJ, INCE/J, and MASJ.